EUV mask feature reconstruction via phase retrieval

Ansuinelli, Paolo; Coene, Wim; Urbach, Paul

DOI
10.1117/12.2525976

Publication date
2019

Document Version
Accepted author manuscript

Published in
Proceedings of SPIE

EUV mask feature reconstruction via phase retrieval

Paolo Ansuinelli[a], Wim Coene[a,b], and Paul Urbach[a]

[a]Optics Research Group, Department of Imaging Physics, Faculty of Applied Sciences, Delft University of Technology, P.O. Box 5046, 2600GA Delft, The Netherlands
[b]ASML Netherlands B.V., De Run 6501, 5504 DR Veldhoven, The Netherlands

ABSTRACT

EUV lithography is the main candidate for patterning of future technology nodes. Its successful implementation depends on many aspects, among which the availability of actinic mask metrology tools able to inspect the patterned absorber in order to control and monitor the lithographic process. In this work, we perform a simulation study to assess the performance of coherent diffractive imaging (CDI) and related phase retrieval methods for the reconstruction of non-trivially shaped and a–periodic nanostructures from far field intensity data.

Keywords: EUV mask metrology, phase retrieval, CDI

1. INTRODUCTION

Moore's law,[1] the prediction that the number of transistor per chip in an integrated circuit doubles every two year, has guided and driven the technological trends and goals of the semiconductor industry since 1965. The aggressive shrinking of electronic devices and components has been a driving force for important technological changes in the lithographic industry. This includes wavelength shrinkage from 436 nm to 193 nm and the introduction of immersion lithography.[2,3] The patterning of future technology nodes requires a further demand in terms of technological development. Extreme ultraviolet lithography is a promising candidate for patterning of sub–10 nm nodes, but its readiness for high volume manufactoring (HVM) relies on the availability of solutions to numerous challenges.[4] Mask metrology represents one of the challenges of EUV lithography. Owing to the high number of atomic resonances in the EUV wavelength region, the optics needs to be reflective. As the result, the usually transmissive lithographic mask is replaced by a Mo/Si multilayer coated reflective mask. The mask is vulnerable to irregularities or defects, such as bumps or pits on the multilayer, that need to be captured during an inspection step, and possibly be avoided or repaired, in order for them not to be printed on wafer. This makes EUV mask inspection and metrology tools essential. As some of the defects are visible only using EUV radiation, the actinic investigation is especially important.[5] Owing to the lack of optics in the EUV portion of the electromagnetic spectrum, lensless imaging via coherent diffractive imaging (CDI) methods is particularly attractive. In CDI, a beam illuminates an object and the scattered light is recorded at the far field. The far field intensity data is then computationally processed to retrieve an image of the scatterer by solving the related phase retrieval problem.[6] This in principle enables aberration–free diffraction–limited imaging.

Retrieving the phase of a scattered wave is a nonlinear, inverse and ill–posed problem. This implies, among other aspects, that there might no be a unique solution to it, or that it might not be easy to find a good solution algorithmically. The challenging mathematical aspects of phase retrieval have stimulated research in the development of methods and algorithms for robust phase retrieval.[7–10] Nevertheless, the most widely employed algorithms are iterative projection methods, in which the guessed wavefront is propagated back and forth among real and Fourier space and constraints in both spaces are employed to guide the estimated phase function towards the true solution.[11–14] Proper sampling of the intensity patterns that are to be processed by the algorithms requires the object to be isolated and this in turn limits the applicability of single intensity iterative phase retrieval methods to isolated samples.[15]

A phase retrieval method that removes this limitation is ptychography.[16] The ptychographic method employs a scanning probe that illuminates an object at overlapping positions. By introducing translation diversity and

E-mail: p.ansuinelli@tudelft.nl

redundancy in the data, ptychography solves an overdetermined set of equations to achieve a wide field of view, high resolution reconstruction of the scattering object. In ptychography light–matter interaction is modeled via a transmission function approach: given a certain illumination function $P(\boldsymbol{r})$ and a certain scattering object $O(\boldsymbol{r})$, the exit wave at a plane placed just afterwards the object is given by $\psi = P(\boldsymbol{r} - \boldsymbol{R})O(r)$. Because the illumination itself acts as a support,[17] proper sampling of the intensity patterns is guaranteed and one can retrieve the phase of the transmission function that describes the object without the need for the object to be isolated. Interestingly, the 2–D multiplicative approximation at the core of the ptychographic method has been found to hold also for objects whose thickness is a multiple of the wavelength,[18] where light confinement and diffraction through the thickness of the material play a role in image formation.[19] Ptychography has been recently employed in the context of actinic mask inspection.[18,20,21]

In this work, we perform a simulation study and we show how single intensity projection–based algorithms - the hybrid input-output (HIO)[6] and the relaxed averaged alternating reflections (RAAR)[13] - and ptychography can be employed to reconstruct the layout of EUV structures on the mask. We use the FEM package JCMSuite[22] and an ASML in–house developed integral Maxwell solver for the generation of far field intensity data.

2. THE METHODS

Phase retrieval methods aim to reconstruct the phase of a certain object, described by the function $f(\mathbf{r}) = |f(\mathbf{r})|e^{i\phi(\mathbf{r})}$, from far field diffraction data, which is related to the object by a Fourier transform $F(\mathbf{u}) = |F(\mathbf{u})|e^{i\psi(\mathbf{u})}$. As only the intensity of the Fourier transform, $|F(\mathbf{u})|^2$, can be recorded all the phase information of the scatterer field is lost. Different methods, iterative or direct, are available to reconstruct such phase. In what follows we outline the steps of the algorithms we have used.

2.1 Hybrid input output (HIO)

The hybrid input output algorithm,[6] makes use of constraints in conjugated planes to drive the reconstruction. The recorded field amplitude $|F(\mathbf{u})|$ is used as a constraint in the Fourier space, while the extension of the object in real space, so called support, is used as a constraint in real space. Information about the dimension of the object in real space is available even without any prior information, as it can be computed by an inverse Fourier of the recorded intensity.[23] The algorithm proceeds by iterated projections among the Fourier and real space.

At the k–th iteration:

1. Given the current estimate of the object $f_k(\mathbf{r})$
2. We Fourier transform $f_k(\mathbf{r})$ to get the estimated diffraction field $F_k(\mathbf{u})$
3. The current guessed Fourier amplitudes $|F_k(\mathbf{u})|$ are replaced by the measured ones, $|F(\mathbf{u})|$, while the phase of the current iterate is retained to get an updated diffracted field $F'(\mathbf{u})$
4. The current Fourier estimate is propagated to the real space by means of an inverse Fourier transform $f'(\mathbf{r})$, and
5. The support constraint, S, is used to get to a revised estimation of the object:

$$f_{k+1}(\mathbf{r}) = \begin{cases} f'_k(\mathbf{r}) & \text{if } \mathbf{r} \in S \\ f_k(\mathbf{r}) - \beta f'_k(\mathbf{r}) & \text{otherwise} \end{cases} \tag{1}$$

In (1) S is defined so to include also the points in which the imaginary part of the object is positive.[14]

2.2 Relaxed Averaged Alternating Reflections (RAAR)

The RAAR algorithm tries to approach the global solution of the phase problem by projecting the current solution to a closed set which is twice as far. This is done introducing the reflector operator $\mathbf{R} = \mathbf{I} + 2(\mathbf{P} - \mathbf{I})$, where $\mathbf{I}$ is the identity operator and $\mathbf{P}$ is the projection operator.[13,24]

Step 5 in the HIO is then replaced by:

$$f_{k+1}(\mathbf{r}) = \begin{cases} f'_k(\mathbf{r}) & \text{if } \mathbf{r} \in S \\ \beta f_k(\mathbf{r}) - (1-2\beta) f'_k(\mathbf{r}) & \text{otherwise} \end{cases} \tag{2}$$

2.3 Ptychography

In ptychography, a set of computed far–field diffraction patterns is processed by certain algorithms to get to an image via phase retrieval. In this work we have used the ptychographical iterative engine (PIE). At the n–th iteration:

1. Given the guessed object $O_{g,n}$,
2. Multiply the current guessed object by the illumination function at position $\mathbf{R}$ to get the guessed exit wave at the current position
$$\psi_{g,n}(\boldsymbol{r},\boldsymbol{R}) = P(\boldsymbol{r}-\boldsymbol{R})O_{g,n}(\boldsymbol{r}) \tag{3}$$
3. Fourier transform the exit wave $\psi_{g,n}(\boldsymbol{r},\boldsymbol{R})$ to get $\Psi_{g,n}(\boldsymbol{k},\boldsymbol{R}) = \mathcal{F}[\psi_{g,n}(\boldsymbol{r},\boldsymbol{R})] = |\Psi_{g,n}|e^{i\theta_{g,n}(\boldsymbol{k},\boldsymbol{R})}$
4. Enforce the measured amplitudes at the far–field on the current far–field guess, to get a corrected guess:
$$\Psi_{c,n}(\boldsymbol{k},\boldsymbol{R}) = |\Psi|e^{i\theta_{g,n}(\boldsymbol{k},\boldsymbol{R})} \tag{4}$$
5. Inverse Fourier transform to get a revised exit wave:
$$\psi_{c,n}(\boldsymbol{r},\boldsymbol{R}) = \mathcal{F}^{-1}[\Psi_{c,n}(\boldsymbol{k},\boldsymbol{R})] \tag{5}$$
6. Update the transmission function of the object in the area covered by the probe by
$$O_{g,n+1} = O_{g,n} + \frac{|P(\boldsymbol{r}-\boldsymbol{R})|}{|P_{max}(\boldsymbol{r}-\boldsymbol{R})|}\frac{P^*(\boldsymbol{r}-\boldsymbol{R})}{(|P^*(\boldsymbol{r}-\boldsymbol{R})|^2+\alpha)}\beta(\psi_{c,n}(\boldsymbol{r},\boldsymbol{R})-\psi_{g,n}(\boldsymbol{r},\boldsymbol{R})) \tag{6}$$
Where α prevents division by zero and β is an appropriately chosen feedback parameter
7. Move the probe to the next position $\boldsymbol{R}$ so that there is sufficiently overlap
8. Repeat 2 to 7 for a sufficient number of iterations

3. NUMERICAL RESULTS

3.1 Single intensity phase retrieval

In the simulation study that follows we employ the methods described above to retrieve the phase of nontrivially shaped isolated nanostructures. The x–polarized EUV radiation illuminates a Mo/Si multilayer coated reflective mask, with a patterned absorber profile on top of it. The angle of incidence is 6°, for which the multilayer is in resonance, giving a reflectance of 60–70% We replace the multilayer with an equivalent substrate that offers, for the given wavelength and angles of incidence, approximately the same reflectance. The incoming light field is a gaussian beam, represented in Figs. 1(a,b), with a 3σ diameter of about $2\mu m$ and radiating 5e11 photons/sec. The detection NA is 0.6. The computational domain, of about $160 \times 160 \times 90nm^3$ is truncated on all sides by the perfectly matched layers and the far field data is sampled so to guarantee an aboundant oversampling ratio (> 10). The materials used for the simulations are reported in Table 1. Computations are performed using the rigorous forward Maxwell solver JCMsuite. At the k–th iteration, an error metric is used to monitor the phase reconstruction:[6,14]
$$E_k = \left(\frac{\sum_{\boldsymbol{r}\notin S}|f'_k(\boldsymbol{r})|^2}{\sum_{\boldsymbol{r}\in S}|f'_k(\boldsymbol{r})|^2}\right)^{1/2} \tag{7}$$

Table 3. Layers thicknesses and material properties at $\lambda = 13.5$ nm

layer	thickness [nm]	n	k
ARC TaBO	2	0.952	0.026
Absorber TaBN	58	0.95	0.031
Ru	0.5	0.88586	0.01727
Ru (Capping layer)	2	0.88586	0.01727
Si	1.8968	0.99888	0.00183
MoSi2	0.7986	0.96908	0.00435
Mo	2.496	0.92347	0.00649
MoSi2	1.8908	0.96908	0.00435

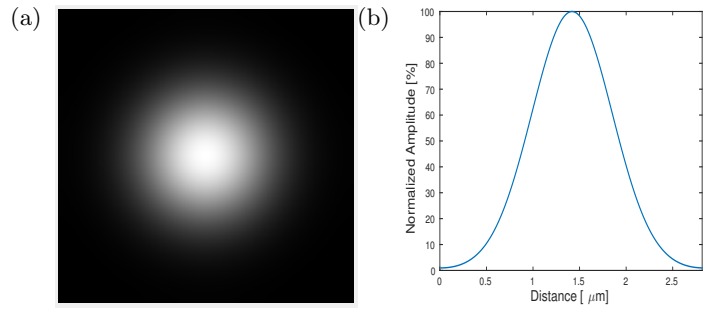

Figure 1. Probe used for the computational experiment. (a) full probe and (b) cross section)

We considered structures of increasing complexity. Figure (1) reports the results for an I–shaped structure, Figure (2) the ones for an L–shaped structure while in Figure (3) we considered a U–shaped structure. The pixel size in the real space has been computed by the theoretical limit $\delta x = \frac{\lambda}{2NA} \approx 11\text{nm}$.

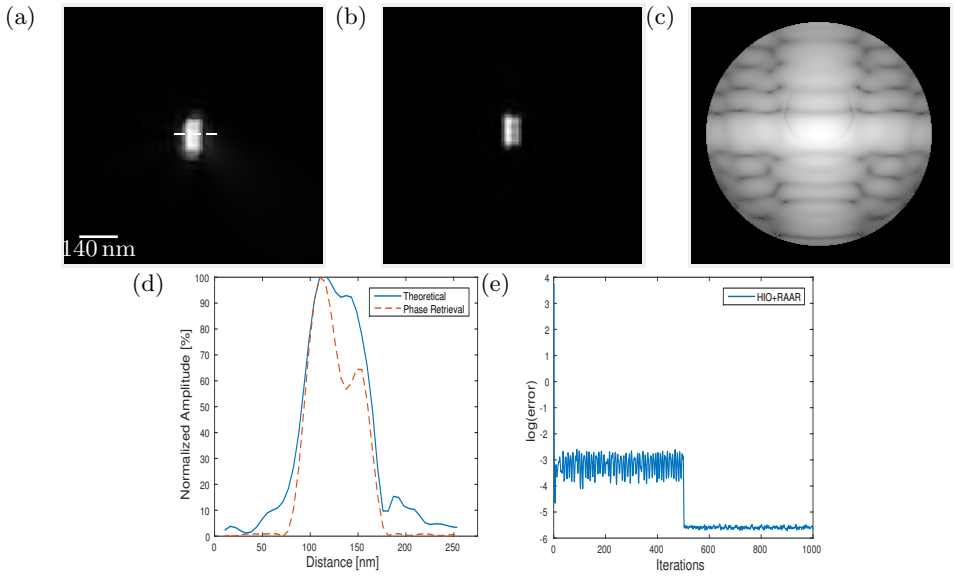

Figure 2. Reconstruction – magnitude – for an I–shaped nanostructure.(a) theoretical object obtained by direction inversion of computed far–field; (b) reconstructed object; (c) far field intensities; (d)cross–section, along the white line in (a), of the theoretical and the reconstructed object and (e)error

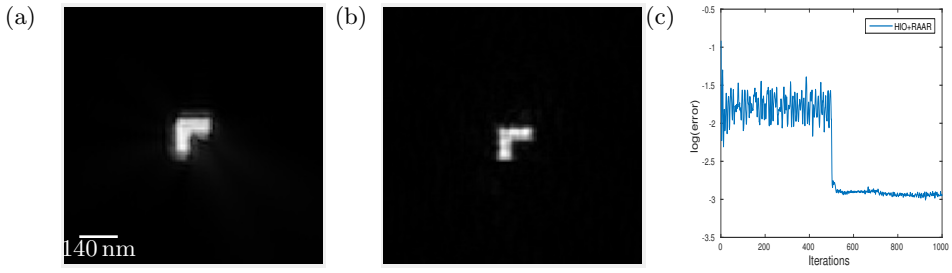

Figure 3. Reconstruction – magnitude – for an L–shaped nanostructure. (a) theoretical object; (b) reconstructed object and (c) error

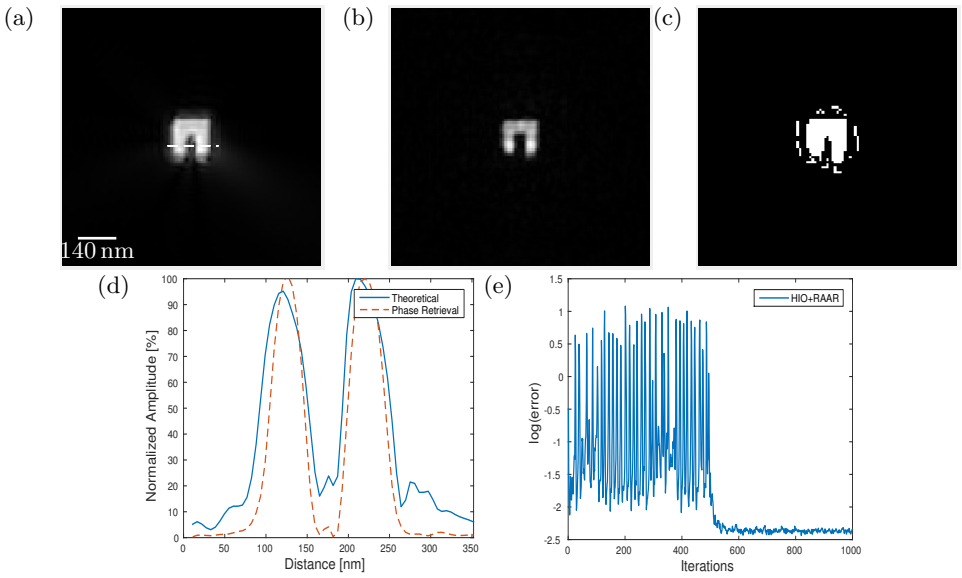

Figure 4. Reconstruction –magnitude – for an U–shaped nanostructure. (a) theoretical object; (b) reconstructed object; (c) support used for the reconstruction; (d) cross–section, along the line in (a), of the theoretical and the reconstructed object and (e) error

The images in Figs. 2–4 have been obtained by aligning and averaging 4 good reconstructions. The feedback parameter β was heuristically set to 0.86. We have added noise for a SNR = 90 dB. The cross sections in Figs. 2 and 3 (d) reveal that the phase retrieval reconstruction mimics closely, albeit with some imperfections, the theoretical object. The retrieval of the I and L–shaped structures did not require any prior information about the shape of the object and a satisfactory retrieval of the phase has been obtained using a loose square support of a certain amount of pixel. Reconstructing the U–shaped structure was more involved and we used prior information about the object, which is generally available in lithography, to generate a suitable support. In this case this was done by finding the edges of Fig 4(a) and filling them with ones. This support is depicted in Fig 4(c).

3.2 Ptychography

In what follows we describe the simulation results we had for actinic ($\lambda = 13.5$ nm) inspection of EUV mask layout. To generate the data for the numerical ptychographic experiment we have used a volume–integral Maxwell Solver, developed in–house at ASML. The solver is formulated for the problem of scattering from periodic objects hence, in order to avoid cross–talk among adjacent cells, we have opted for a super–cell approach. The cell size is $\Lambda = 3.5\mu m$. The sampling in the far field and in the illuminating NA equals $\frac{2\pi}{\Lambda}$. The probe is described by its angular spectrum and the plane waves which compose the illumination are evaluated one at a time in parallel on a multicore HPC cluster. The output of the probe is then given by the coherent superposition of the separated contributions. The shifts are performed shifting the object of 0.2 μm inside the supercell. The probe is polarized in the x direction by proper linear combination of s and p polarization states.

Although the sample is very complex, with a thickness of the structures which is about 5–6 times the wavelength, and although the data has been generated by rigorously solving Maxwell' s equations in a reflective setting, the scalar ptychographic transmission function approach has been found to be sufficient to properly reconstruct the layout of the EUV absorber (Fig.5).

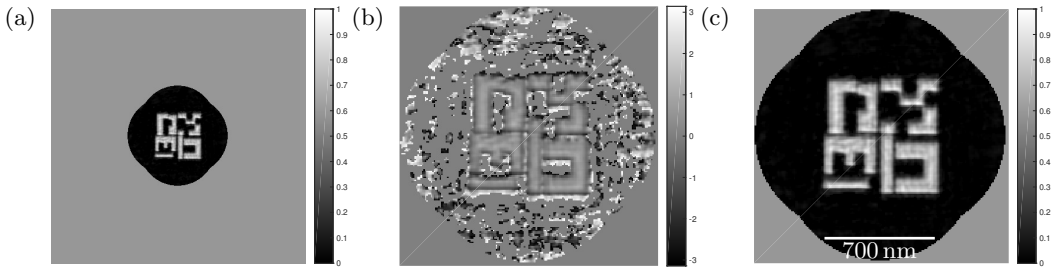

Figure 5. (a)Ptychographic reconstruction – magnitude – of an ensemble of nanostructures. (b)Phase of the reconstruction. (c) Zoom of (a)

Some of the distances among structures are of the order of the wavelength and they appear quite resolved in the final image 5(a–c).

4. CONCLUSIONS

Mask metrology and inspection tools are essential for the successful implementation of EUV lithography. The lack of optics for EUV radiation makes lensless imaging a natural candidate for the purpose. In this work, we have studied, by means of rigorous simulations, the performance of single intensity phase retrieval algorithms and ptychography for the imaging of EUV patterned absorber layouts. The results show satisfactory reconstructions of isolated nontrivially shaped nanostructures and also of ensembles of nanostructures. The study demonstrates the potentiality of CDI methods for the inspection of EUV masks.

ACKNOWLEDGMENTS

We acknowledge Sven Burger and the JCMwave team for providing access to the JCM solver. We are grateful to Mark Van Kraaij, ASML, for assistance with the use of the volume–integral Maxwell solver.

The authors acknowledge financial support from the European Union's Horizon 2020 research and innovation program under the Marie Skłodowska-Curie Grant Agreement No. 675745.

REFERENCES

[1] Schaller, R. R., "Moore's law: Past, present, and future," *IEEE Spectr.* **34**, 52–59 (jun 1997).

[2] Rothschild, M., Goodman, R. B., Hartney, M. A., Horn, M. W., Kunz, R. R., Sedlacek, J. H. C., and Shaver, D. C., "Photolithography at 193 nm," *Journal of Vacuum Science & Technology B: Microelectronics and Nanometer Structures Processing, Measurement, and Phenomena* **10**(6), 2989–2996 (1992).

[3] Lin, B.-J., "Immersion lithography and its impact on semiconductor manufacturing," *Journal of Micro/Nanolithography, MEMS, and MOEMS* **3**(3), 377 – 500 – 124 (2004).

[4] Bakshi, V., [*EUV lithography*], vol. PM2814, SPIE Press (2 2018).

[5] Rajendran, R., Mochi, I., Helfenstein, P., Mohacsi, I., Redford, S., Mozzanica, A., Schmitt, B., Yoshitake, S., and Ekinci, Y., "Towards a stand-alone high-throughput euv actinic photomask inspection tool: Rescan," in [*Proc. SPIE 10145, Metrology, Inspection, and Process Control for Microlithography XXXI*], **10145** (2017).

[6] Fienup, J. R., "Phase retrieval algorithms: a comparison," *Appl. Opt.* **21**, 2758–2769 (Aug 1982).

[7] Shechtman, Y., Eldar, Y. C., Cohen, O., Chapman, H. N., Miao, J., and Segev, M., "Phase retrieval with application to optical imaging: A contemporary overview," *IEEE Signal Processing Magazine* **32**, 87–109 (May 2015).

[8] Candes, E. J., Strohmer, T., and Voroninski, V., "Phaselift: exact and stable signal recovery from magnitude measurements via convex programming," *Communications on Pure and Applied Mathematics* **66**(8), 1241–1274 (2013).

[9] Cands, E., Eldar, Y., Strohmer, T., and Voroninski, V., "Phase retrieval via matrix completion," *SIAM Journal on Imaging Sciences* **6**(1), 199–225 (2013).

[10] Beck, A. and Eldar, Y., "Sparsity constrained nonlinear optimization: Optimality conditions and algorithms," *SIAM Journal on Optimization* **23**(3), 1480–1509 (2013).

[11] GERCHBERG, R. W., "A practical algorithm for the determination of phase from image and diffraction plane pictures," *Optik* **35**, 237 (1972).

[12] Fienup, J. R., "Phase retrieval algorithms: a personal tour," *Appl. Opt.* **52**, 45–56 (Jan 2013).

[13] Luke, D. R., "Relaxed averaged alternating reflections for diffraction imaging," *Inverse Problems* **21**, 37–50 (nov 2004).

[14] Miao, J., Sayre, D., and Chapman, H. N., "Phase retrieval from the magnitude of the fourier transforms of nonperiodic objects," *J. Opt. Soc. Am. A* **15**, 1662–1669 (Jun 1998).

[15] Sayre, D., "Some implications of a theorem due to shannon," *Acta Crystallographica* **5**(6), 843–843 (1952).

[16] Rodenburg, J. M. and Faulkner, H. M. L., "A phase retrieval algorithm for shifting illumination," *Applied Physics Letters* **85**(20), 4795–4797 (2004).

[17] Konijnenberg, A., Coene, W., Pereira, S., and Urbach, H., "Combining ptychographical algorithms with the hybrid input-output (hio) algorithm," *Ultramicroscopy* **171**, 43 – 54 (2016).

[18] Helfenstein, P., Rajeev, R., Mochi, I., Kleibert, A., Vaz, C. A. F., and Ekinci, Y., "Beam drift and partial probe coherence effects in euv reflective-mode coherent diffractive imaging," *Opt. Express* **26**, 12242–12256 (Apr 2018).

[19] Zayko, S., Mönnich, E., Sivis, M., Mai, D. M., Salditt, T., Schäfer, S., and Ropers, C., "Coherent diffractive imaging beyond the projection approximation: waveguiding at extreme ultraviolet wavelengths.," *Optics express* **23 15**, 19911–21 (2015).

[20] Mochi, I., Helfenstein, P., Rajeev, R., Fernández, S., Kazazis, D., Yoshitake, S., and Ekinci, Y., "Actinic inspection of euv reticles with arbitrary pattern design," in [*Photomask Technology*], (2017).

[21] Fernandez, S., Kazazis, D., Rajendran, R., Mochi, I., Helfenstein, P., Yoshitake, S., and Ekinci, Y., "Comparative study of extreme ultraviolet absorber materials using lensless actinic imaging," *Journal of Micro/Nanolithography, MEMS, and MOEMS* **18**(1), 1 – 6 – 6 (2019).

[22] https://jcmwave.com/.

[23] Marchesini, S., He, H., Chapman, H., Hau-Riege, S., Noy, A., Howells, M., Weierstall, U., and Spence, J., "X-ray image reconstruction from a diffraction pattern alone," *Physical Review B-Condensed Matter* **68**, 1401011–1401014 (10 2003).

[24] Marchesini, S., "Invited article: A unified evaluation of iterative projection algorithms for phase retrieval," *Review of Scientific Instruments* **78**(1), 011301 (2007).